AN ADAPTIVE N-FIDELITY METAMODEL FOR DESIGN AND OPERATIONAL-UNCERTAINTY SPACE EXPLORATION OF COMPLEX INDUSTRIAL PROBLEMS

A. SERANI*, R. PELLEGRINI*, R. BROGLIA*, J. WACKERS†, M. VISONNEAU†, AND M. DIEZ*

*CNR-INM, National Research Council-Institute of Marine Engineering
Via di Vallerano 139, 00128 Rome, Italy
e-mail: {andrea.serani, riccardo.pellegrini}@inm.cnr.it, {riccardo.broglia, matteo.diez}@cnr.it

†LHEEA Lab, Ecole Centrale de Nantes, CNRS-UMR
6598, 44321 Nantes Cedex 3, France
e-mail: {jeroen.wackers, michel.visonneau}@ec-nantes.fr

Key words: Multi-fidelity, adaptive metamodels, simulation-based design optimization, uncertainty quantification, adaptive-grid refinement, multi-grid acceleration

Abstract. An adaptive N-fidelity (NF) metamodel is presented for the solution of simulation-based design optimization and uncertainty quantification problems. A multi-fidelity approximation is built by an additive correction of a low-fidelity metamodel with metamodels of hierarchical differences (errors) between higher-fidelity levels. The metamodel is based on the expected value of an ensemble of stochastic radial-basis functions, which also provides the uncertainty associated to the prediction. New training points are added to the appropriate fidelity level, based on the NF prediction uncertainty and the computational cost. The method is demonstrated for an analytical test function, the shape optimization of a NACA hydrofoil, and the operational-uncertainty quantification of a RoPax ferry. The fidelity levels are defined by adaptive-grid refinement and multi-grid approach, for the NACA hydrofoil and the RoPax ferry, respectively. The generalization of the multi-fidelity concept to N fidelities shows promising results both in terms of accuracy and computational cost.

1 INTRODUCTION

Ship performance depends on design and operational (including environmental) parameters. The accurate prediction of significant design metrics (such as resistance and powering requirements; seakeeping, maneuverability, and dynamic stability; structural response and failure) requires prime-principle-based high-fidelity computational tools (e.g., for computational fluid/structural dynamics, CFD/EFD), especially for innovative configurations and off-design conditions. These tools are generally computationally expensive, making the exploration of design (such as in simulation-based design optimization, SBDO) and operational-uncertainty (such as in uncertainty

quantification, UQ) spaces a technological challenge.

To reduce the computational cost of SBDO and UQ processes, metamodeling methods have been developed and successfully applied in several engineering fields [1]. Among other metamodels, radial basis functions (RBF) methods have demonstrated their accuracy and efficiency in engineering design [2]. Further efficiency is gained using dynamic metamodels, for which the design of experiments (DoE) for metamodel training is not defined a priori but dynamically updated, exploiting the information that becomes available during the analysis process. Thus, training points are added where it is most useful, reducing the number of function evaluations required to properly represent the function. An adaptive sampling criterion based on the maximum prediction uncertainty for dynamic radial basis functions (DRBF) has been presented by [3]. Other sampling approaches are based on the expected improvement [4] and multi-criteria adaptive sampling [5].

In addition to dynamic metamodels, multi-fidelity approximation methods have been developed to further reduce the cost of the SBDO procedure, combining the accuracy of high-fidelity solvers with the computational cost of low-fidelity solvers. Multi-fidelity (MF) metamodels use mainly low-fidelity simulations and few high-fidelity (accurate, expensive) simulations used to preserve the accuracy of the overall model. Several metamodels have been used in the literature with MF data, like non-intrusive polynomial chaos [6], co-kriging [7] and RBF [8]. In SBDO based on CFD computations, high- and low-fidelity evaluations may be obtained by varying the physical model, the size of the computational grid, and/or combining experimental data with numerical simulations [9]. Most MF approaches generally use two fidelity levels.

The objective of the present work is to formulate and assess an N-fidelity (NF) metamodel for design and operational-uncertainty space exploration of complex industrial problems.

The NF metamodel is developed as an extension of the authors' previous work [10]. The methodology is tested on a 1-D analytical problem and then applied to: (i) the shape optimization of a NACA hydrofoil and (ii) the uncertainty quantification of a roll-on/roll-off passengers (RoPax) ferry. CFD computations are based on two unsteady Reynolds averaged Navier-Stokes equations (RANSE) solvers: (1) ISIS-CFD [11], developed at Ecole Centrale de Nantes/CNRS and integrated in the FINE/Marine simulation suite from NUMECA Int, for the SBDO problem; (2) χnavis [12], developed at CNR-INM, for the UQ problem. In ISIS-CFD, mesh deformation and adaptive grid refinement techniques are adopted to allow the automatic shape deformation of the hydrofoil. The fidelity levels are defined by the grid refinement ratio. In χnavis, different fidelities are obtained using multi-grids.

2 N-FIDELITY METAMODEL

Consider $\mathbf{x} \in \mathbb{R}^D$ as the design and/or operational uncertainty vector of dimension D. Let the true function $f(\mathbf{x})$ be assessed by MF simulations: the highest-fidelity level is $f_1(\mathbf{x})$, the lowest-fidelity is $f_N(\mathbf{x})$, and arbitrary intermediate fidelity levels are $\{f_i\}_{i=2}^{N-1}(\mathbf{x})$. Let training sets be available for each level: $\{\mathcal{T}_i\}_{i=1}^{N} = \{\mathbf{x}_j, f_i(\mathbf{x}_j)\}_{j=1}^{J_i}$, with $\{J_i\}_{i=1}^{N}$ the training set size. Then an intra-level error $\varepsilon_i(\mathbf{x}) = f_i(\mathbf{x}) - f_{i+1}(\mathbf{x})$ can be defined with an associate training set $\mathcal{E}_i = \{(\mathbf{x}, f_i(\mathbf{x}) - f_{i+1}(\mathbf{x})) \,|\, \mathbf{x} \in \mathcal{T}_i \cap \mathcal{T}_{i+1}\}$.

Using these sets, metamodels $\tilde{f}_N$ and $\{\tilde{\varepsilon}_i\}_{i=1}^{N-1}$ are trained, where "$\sim$" denotes metamodel prediction based on a stochastic ensemble of radial basis functions, which also provides the

prediction uncertainty U. Assuming the uncertainty associated to the prediction of the lowest-fidelity $U_{\tilde{f}_N}$ and intra-level errors $U_{\tilde{\varepsilon}_i}$ as uncorrelated, the NF approximation $\hat{f}(\mathbf{x})$ of $f(\mathbf{x})$ and its uncertainty $U_{\hat{f}}$ reads

$$\hat{f}(\mathbf{x}) = \tilde{f}_N(\mathbf{x}) + \sum_{i=1}^{N-1} \tilde{\varepsilon}_i(\mathbf{x}) \qquad \text{and} \qquad U_{\hat{f}}(\mathbf{x}) = \sqrt{U^2_{\tilde{f}_N}(\mathbf{x}) + \sum_{i=1}^{N-1} U^2_{\tilde{\varepsilon}_i}(\mathbf{x})} \tag{1}$$

The contribution of each fidelity level to $U_{\hat{f}}$ is assessed and used to refine adaptively the training sets as the sampling of the design/operational space progresses.

2.1 Adaptive sampling method

The NF metamodel is dynamically updated by iteratively adding a new training point following a two-step procedure (see Fig. 1): firstly, the coordinates of the new training point $\mathbf{x}^\star$ are identified based on the metamodel maximum uncertainty [10], solving the single-objective maximization problem:

$$\mathbf{x}^\star = \underset{\mathbf{x}}{\text{argmax}}[U_{\hat{f}}(\mathbf{x})]. \tag{2}$$

secondly, once $\mathbf{x}^\star$ is identified, either $\mathcal{T}_N$ or all the training sets from $\mathcal{T}_k$ to $\mathcal{T}_{k+1}$ are refined according to Eq. 3. Defining $\beta_i = c_{i+1}/c_i$, $i = 1, ..., N-1$, where c_i is the computational cost associated to the i-th level, $\mathbf{U} \equiv \{\beta_1 U_{\tilde{\varepsilon}_1}, ..., \beta_{N-1} U_{\tilde{\varepsilon}_{N-1}}, U_{\tilde{f}_N}\}$ as the metamodel uncertainty vector, and $k = \text{maxloc}(\mathbf{U})$:

$$\begin{cases} \text{If } k = N & \text{add } \{\mathbf{x}^\star, f_N(\mathbf{x}^\star)\} \text{ to } \mathcal{T}_N, \\ \text{else,} & \text{add } \{\mathbf{x}^\star, f_i(\mathbf{x}^\star)\} \text{ to } \mathcal{T}_i \;\; \text{with} \;\; i = k, k+1 \end{cases} \tag{3}$$

In the first case, only the lowest-fidelity evaluation is performed, whereas two evaluations are required at the same $\mathbf{x}^\star$ in the second case.

2.2 Stochastic radial basis functions

The metamodel prediction $\tilde{f}(\mathbf{x})$ is computed as the expected value (EV) over a stochastic tuning parameter of the RBF metamodel, $\tau \sim \text{unif}[1, 3]$:

$$\widetilde{f}(\mathbf{x}) = \text{EV}\left[g(\mathbf{x}, \tau)\right]_\tau, \quad \text{with} \quad g(\mathbf{x}, \tau) = \sum_{j=1}^{J} w_j ||\mathbf{x} - \mathbf{x}_j||^\tau, \tag{4}$$

where w_j are unknown coefficients, $||\cdot||$ is the Euclidean norm. The coefficients w_j are determined enforcing exact interpolation at the training points $g(\mathbf{x}_j, \tau) = f(\mathbf{x}_j)$ by solving $\mathbf{A}\mathbf{w} = \mathbf{f}$, with $\mathbf{w} = \{w_j\}$, $a_{lj} = ||\mathbf{x}_l - \mathbf{x}_j||^\tau$ and $\mathbf{f} = \{f(\mathbf{x}_j)\}$.

The uncertainty $U_{\widetilde{f}}(\mathbf{x})$ associated with the stochastic RBF metamodel prediction is quantified by the 95%-confidence interval of $g(\mathbf{x}, \tau)$, evaluated using a Monte Carlo sampling over τ [3].

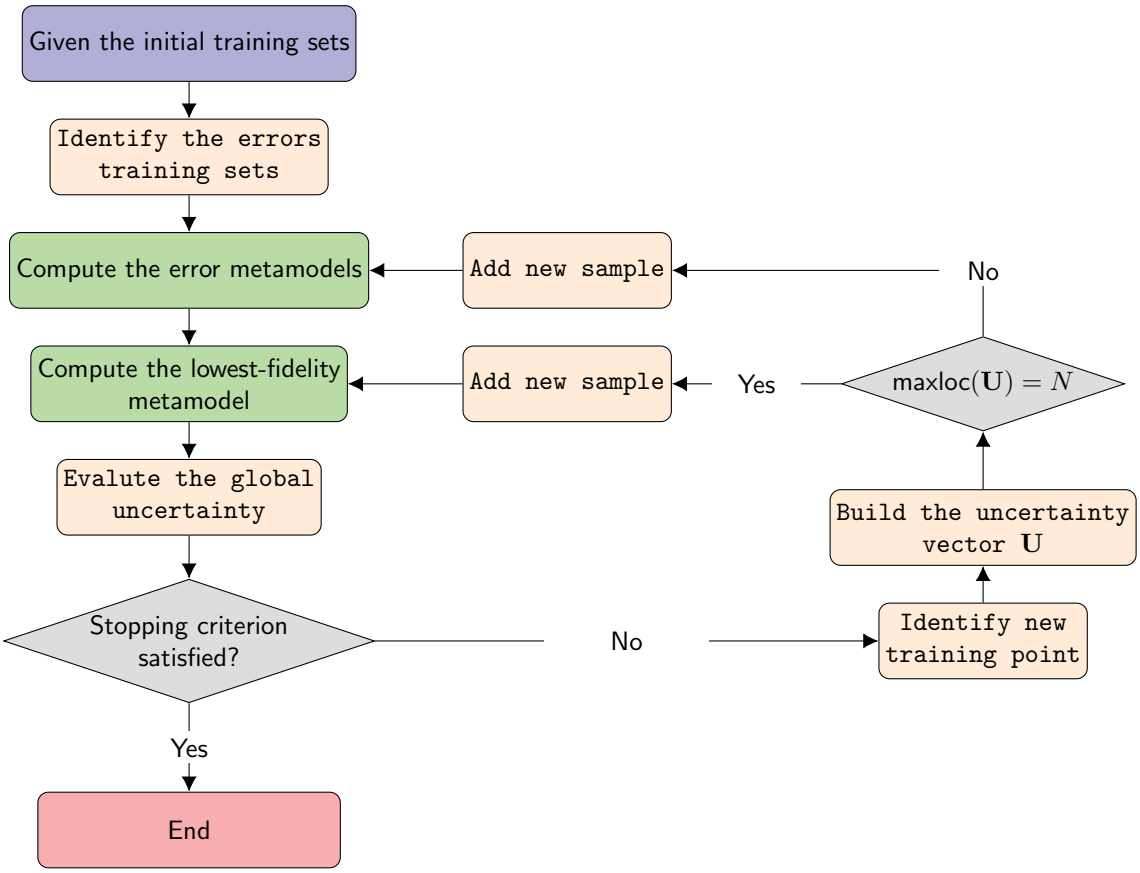

Figure 1: N-fidelity adaptive sampling procedure.

3 ANALYTICAL TEST

One analytical test problem is selected to assess the adaptive NF metamodel performance. It is mono-dimensional and multi-modal. Figure 2a shows the highest-fidelity level (f_1), whereas Figs. 2b and c show, respectively, the same analytical function along with one (f_2) and two ($f_{2,3}$) lower-fidelities and the corresponding errors ($\varepsilon_{1,2}$). The analytical test is defined in Tab. 1.

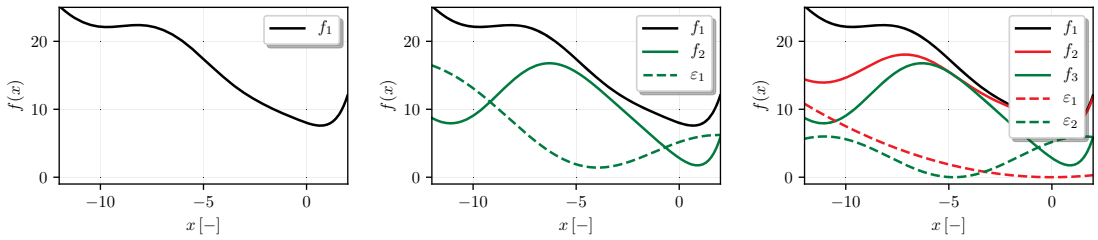

(a) $N = 1$ (b) $N = 2$ (c) $N = 3$

Figure 2: Analytical test problem with different number of fidelities N.

Table 1: Analytical test problem.

N			**Problem**	**Domain**
1	$f_1(x)$	=	$-0.5x(\sin(0.25x)\cos(0.5x)+1-e^x+2.0)+8$	$[-12,2]$
2	$f_1(x)$	=	$-0.5x(\sin(0.25x)\cos(0.5x)+1-e^x+2.0)+8$	
	$f_2(x)$	=	$f_1(x)-\varepsilon_1(x)$	$[-12,2]$
	$\varepsilon_1(x)$	=	$0.075(x)^2+3\cos(0.5x-0.76)+3$	
3	$f_1(x)$	=	$-0.5x(\sin(0.25x)\cos(0.5x)+1-e^x+2.0)+8$	
	$f_2(x)$	=	$f_1(x)-\varepsilon_1(x)$	
	$f_3(x)$	=	$f_2(x)-\varepsilon_2(x)$	$[-12,2]$
	$\varepsilon_1(x)$	=	$0.075x^2$	
	$\varepsilon_2(x)$	=	$3\cos(0.5x-0.76)+3$	

4 NACA HYDROFOIL SHAPE OPTIMIZATION PROBLEM

This problem addresses the drag minimization of a NACA four-digit airfoil. The following minimization problem is solved

$$\begin{aligned} \text{minimize} \quad & C_D(\mathbf{x}) \\ \text{subject to} \quad & C_L(\mathbf{x}) = 0.6 \\ \text{and to} \quad & \mathbf{l} \leq \mathbf{x} \leq \mathbf{u} \end{aligned} \tag{5}$$

where $\mathbf{x}$ is the design variable vector, C_D and C_L are respectively the drag and lift coefficient, and $\mathbf{l}$ and $\mathbf{u}$ are the lower and upper bound of $\mathbf{x}$. The equality constraint on the lift coefficient is necessary in order to compare different geometries at the same lift force (typically equal to the weight of the object), since the drag depends strongly on the lift.

The hydrofoil shape (see Fig. 3) is defined by the general equation for four-digit NACA foils. The upper (y_u) and lower (y_l) hydrofoil surfaces are computed as

$$\begin{cases} \xi_u = \xi - y_t \sin\theta \\ \xi_l = \xi + y_t \sin\theta \\ y_u = y_c + y_t \cos\theta \\ y_l = y_c - y_t \cos\theta \end{cases} \quad \text{with} \quad y_c = \begin{cases} \dfrac{m}{p^2}\left[2p\dfrac{\xi}{c} - \left(\dfrac{\xi}{c}\right)^2\right], & 0 \leq \xi < pc \\ \dfrac{m}{(1-p)^2}\left[(1-2p) + 2p\dfrac{\xi}{c} - \left(\dfrac{\xi}{c}\right)^2\right], & pc \leq \xi \leq c \end{cases} \tag{6}$$

where ξ is the position along the chord, c the chord length, y_c the mean camber line, p the location of the maximum camber, m the maximum camber value, and y_t the half thickness

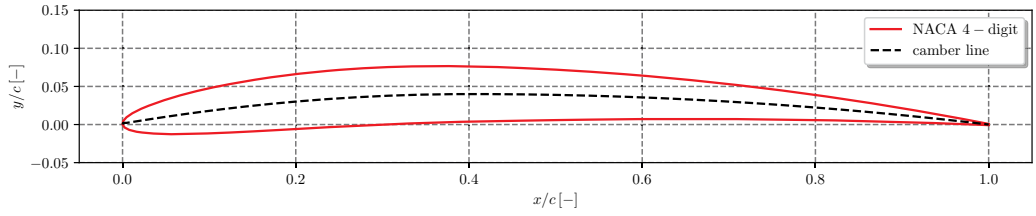

Figure 3: NACA 4-digit hydrofoil.

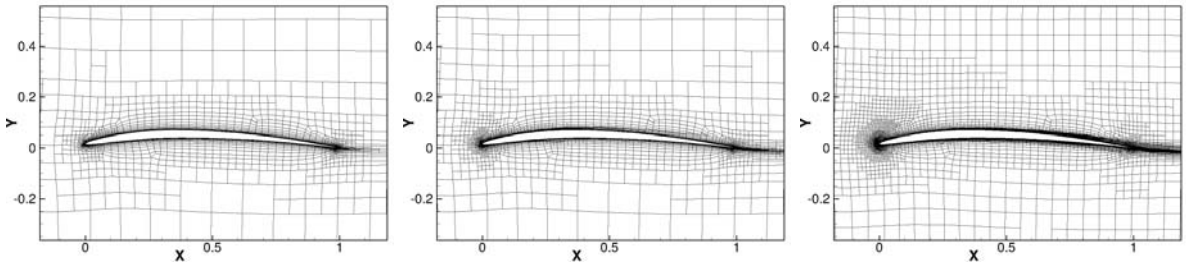

(a) Coarse grid, 3.6k cells (b) Medium grid, 5.7k cells (c) Fine grid, 12.8k cells

Figure 4: NACA hydrofoil computational grids.

given by

$$y_t = 5t\left(0.2969\sqrt{\xi} - 0.1260\xi - 0.3516\xi^2 + 0.2843\xi^3 - 0.1015\xi^4\right) \tag{7}$$

In this work, the design variables vector is defined as $\mathbf{x} = \{t, m\}$ with $t \in [0.030, 0.120]$ and $m \in [0.025, 0.065]$. The maximum camber position is fixed at $p = 0.4$. The simulation conditions are: velocity $U = 10$ m/s, chord $c = 1$ m, fluid density $\rho = 1,026$ kg/m^3, and Reynolds number $\mathrm{Re} = 8.41 \cdot 10^6$.

CFD simulations are performed with the unstructured finite-volume RANSE solver ISIS-CFD developed at ECN – CNRS [11], available in the FINE$^{\mathrm{TM}}$/Marine computing suite from NUMECA Int. Computational grids are created through adaptive grid refinement [13, 14] to take into account the need for high and low fidelity. The simulation strategy in the context of metamodel creation is explained by [10]. The adaptive grid refinement method adjusts the computational grid locally, during the computation, by dividing the cells of an original coarse grid, to improve the precision. The decision where to refine comes from a refinement criterion, a tensor field $\mathcal{C}(x, y, z)$ computed from the flow. The tensor is based on the water surface position and on second derivatives of pressure and velocity. The mesh is refined until the dimensions $\mathbf{d}_{p,j}$ $(j = 1, 2, 3)$ of each hexahedral cell p satisfy

$$\|\mathcal{C}_p \mathbf{d}_{p,j}\| = T_r \tag{8}$$

The refinement criterion based on the second derivatives of the flow is not very sensitive to grid refinement [14], so the cell sizes everywhere are proportional to the constant threshold T_r.

For NF optimization, the interest of this procedure is that different fidelity results can be obtained by running the same simulations with different thresholds T_r. Herein, three fidelity are used. The initial computational grid has 2,654 cells, the refinement threshold value T_r is set equal to 0.1, 0.2, and 0.4 from highest- to lowest-fidelity. The actual computational grids have 12.8, 5.7, and 3.7k cells, respectively (see Fig. 4). Highest- to lowest-fidelity simulations require about 17, 9, and 5 minutes, respectively, of wall-clock time to converge. The resulting computational cost ratios are about $\beta_1 = 0.5$ and $\beta_2 = 0.3$.

The domain runs from $11c$ in front of the leading edge to $16c$ behind the hydrofoil and from $-10c$ to $10c$ vertically. Dirichlet conditions on the velocity are imposed, except on the outflow side which has an imposed pressure condition. The hydrofoil surface is treated with a wall law and $y^+ = 60$ for the first layer. Turbulence is modeled with the standard $k - \omega$ SST model.

To maintain a constant lift (see Eq. 5), the angle of incidence α for the hydrofoil is adjusted dynamically during the simulations.

The budget is defined in terms of normalized computational cost and is equal to 22. The initial training set for the problem is a set of $2N + 1$ points including the domain center and min/max coordinates for each variable. All fidelities are sampled in these points.

5 ROPAX UNCERTAINTY QUANTIFICATION PROBLEM

This problem addresses the UQ of a RoPax ferry in terms of estimation of expected value (EV) and standard deviation (SD) of the (model-scale) resistance (R_T), subject to operational uncertainty. Specifically, the uncertain parameter is the Froude number with a uniform probability density function from 0.25 to 0.35. The RoPax ferry is characterized by: length between perpendicular $L_{\text{PP}} = 162.85$ m, displacement (DWT) of $5,000$ t, block coefficient $C_B = 0.5677$. The analysis is performed with a scale factor $\lambda = 27.14$. The parametric geometry of the RoPax is produced with the computer-aided design (CAD) environment integrated in the CAESES® software, developed by FRIENDSHIP SYSTEMS AG, and made available in the framework of the H2020 EU Project Holiship.

The hydrodynamics performance of the RoPax is assessed by the unsteady RANSE code χnavis developed at CNR-INM. It is based on finite volume scheme, with variable co-located at cell centers. Turbulent stresses are taken into account by the Boussinesq hypothesis, with Spallart-Almaras turbulence model. Free-surface effects are taken into account by a single-phase level-set algorithm. Wall-functions are not adopted, therefore $y^+ = 1$ is ensured on the wall. On solid walls, the velocity is set equal to zero and zero normal gradient is enforced on the pressure field; at the (fictitious) inflow boundary, velocity is set to the undisturbed flow value and the pressure is extrapolated from the inside; the dynamic pressure is set to zero at the outflow, whereas the velocity is extrapolated from inner points. On the top boundary, which remains always in the air region, fluid dynamic quantities are extrapolated from inside. Chimera overlapping grid capabilities are used, the numerical solutions are computed by means of a full multi grid–full approximation scheme (FMG–FAS), with four grid levels (from coarser to finer: G4, G3, G2, and G1), each obtained from the next finer grid with a refinement ratio equal to 2, resulting in $\beta_1 = 0.125$ and $\beta_2 = 0.0625$. In the FMG–FAS approximation procedure, the

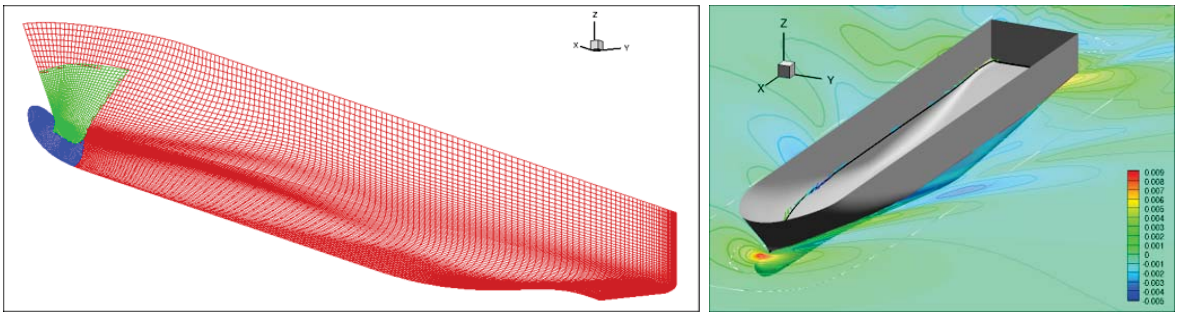

(a) CFD hull grid

(b) Non-dimensional wave elevation, Fr = 0.245

Figure 5: RoPax ferry.

solution is computed on the coarsest grid level first. Secondly, it is approximated on the next finer grid and the solution is iterated by exploiting all the coarser grid levels available with a V-Cycle. The process is repeated up to the finest grid level. For the present UQ problem G1, G2, and G3 grids are used. Simulations are performed considering a water density $\rho = 998.2$ kg/m^3, cinematic viscosity $\nu = 1.105$E-6 m^2/s, gravitational acceleration $g = 9.81$ m/s. The grid is composed by 53 blocks, for a total of 4.88 M cells, see Fig. 5; the domain extends to $2L_{\text{PP}}$ in front of the hull, $3L_{\text{PP}}$ behind, and $1.5L_{\text{PP}}$ each side; a depth of $2L_{\text{PP}}$ is imposed.

6 NUMERICAL RESULTS

The normalized computational cost is defined as 1 for each f_1 evaluation and β_i, $i = 1, ..., N-1$ for each f_{i+1} evaluation. It is worth noting that, the normalized computational cost for the CFD problems is defined, considering only the cost of the highest-fidelity level sampled. This is due to the fact that, adaptive grid refinement and FMG–FAS compute the solution at grid level k using solutions from grid level N to k.

The DPSO algorithm presented in [15] is used for the solution of Eqs. 2 and 5.

6.1 Analytical test problem

The performance of the adaptive NF metamodel is assessed in terms of convergence of the normalized root mean square error (NRMSE), the objective function minimum, and the number of highest-fidelity evaluations, as shown in Fig.6.

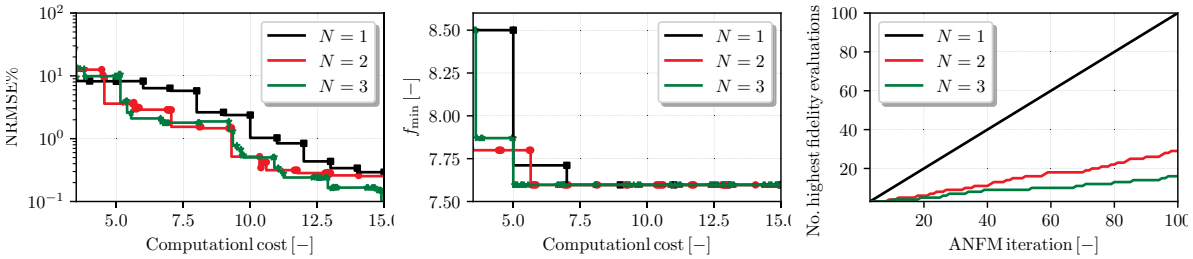

(a) (b) (c)

Figure 6: Analytical test problem: convergences of (a) NRMSE, (b) objective function minimum, and (c) the number of the highest-fidelity evaluations versus the sampling procedure iterations.

It is worth noting that for $N = 3$ the NRMSE decreases faster than for $N = 2$ and $N = 1$, achieving an NRMSE = 0.01% with the lowest computational cost (see Fig.6a). Similarly, for $N = 3$ the minimum of the objective function is achieved with the lowest computational cost (see Fig. 6b). Finally, Fig. 6c shows the number of highest-fidelity evaluations versus the sampling iteration number. It is worth noting that adding intermediate-fidelity levels decreases the need for highest-fidelity samples.

6.2 NACA hydrofoil shape optimization

Figure 7 shows the training sets at the last iteration of the MF metamodel training for $N = 1$, 2, and 3. For $N = 1$ the training points are evenly distributed. For $N = 2$ the low-fidelity

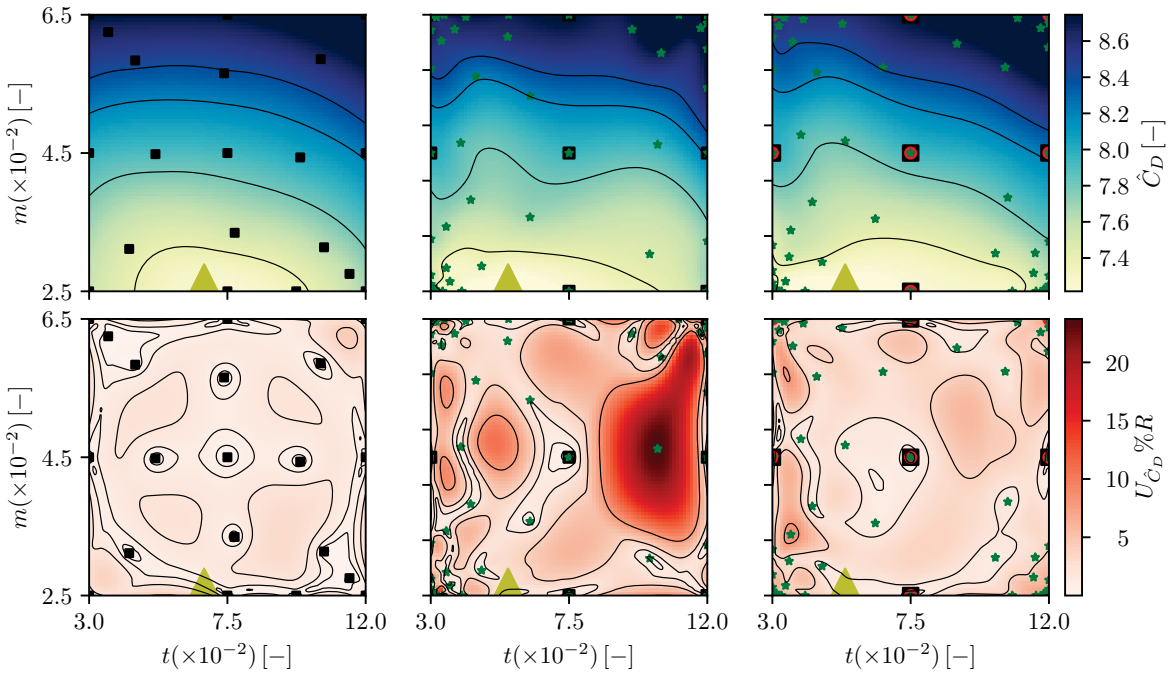

Figure 7: NACA hydrofoil: N-fidelity metamodel prediction and associated uncertainty, with $N = 1$, 2, and 3 from left to right. Black squares, red circles, and green stars are the $i = 1$, 2, and 3 fidelity training sets. Yellow triangles is the minimum position.

evaluations are clustered in three corners. Furthermore, in the latter case the uncertainty of the prediction is significantly higher than for the $N = 1$ case, suggesting the presence of numerical noise. Finally, for $N = 3$ the contour plot of the drag coefficient and the uncertainty look smoother than for $N = 2$. This suggests a regularization effect stemming from the use of a mid-level fidelity. At each iteration the predicted minimum is verified through an highest-fidelity simulation. Fig. 8 shows the convergence of the verified objective function. It is worth noting that the NF metamodel converges faster for both $N = 2$ and 3. Table 2 summarizes, the training sets size, the normalized cost, the maximum uncertainty of the prediction, the coordinates of the predicted minimum of the C_D, the predicted minimum, its verification, the prediction error, and the improvement with respect to the original configuration. It is worth noting that for

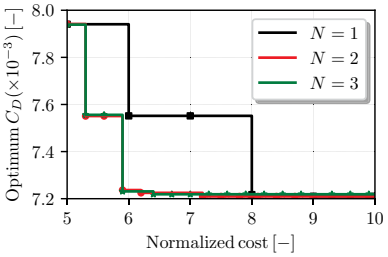

Figure 8: NACA hydrofoil: verified optimum convergence versus the normalized computational cost.

Table 2: Summary of the adaptive NF metamodel performance on the NACA hydrofoil SBDO problem.

				Normalized		minimum position		minimum value			
N	$\lvert\mathcal{T}_1\rvert$	$\lvert\mathcal{T}_2\rvert$	$\lvert\mathcal{T}_3\rvert$	cost	$\max(U_{\hat{f}})\%$	$t\,[-]$	$m\,[-]$	$\widehat{C}_D\,[-]$	$C_D\,[-]$	E%	$\Delta C_D\%$
1	22			22.0	3.70	6.743E-2	0.000E-2	7.209E-3	7.206E-3	0.1	9.23
2	8		46	21.8	23.7	5.515E-2	0.000E-2	7.064E-3	7.209E-3	2.0	9.19
3	5	9	55	20.8	8.78	5.367E-2	0.000E-2	7.094E-3	7.219E-3	1.7	9.07

$N = 3$ the number of highest-fidelity evaluations decreases compared to $N = 1$ and 2. Similar improvements are achieved using $N = 1$, 2, and 3.

6.3 RoPax uncertainty quantification

The NF metamodel for UQ is assessed through statistical estimation of the expected value (EV) and standard deviation (SD) of the total resistance, R_T. The training of the NF metamodel is performed considering at most 4 high-fidelity evaluations. The results are compared to the available highest-fidelity CFD data. Figure 9 shows the MF prediction of the total resistance versus the Froude number, with N =1, 2, and 3. It is worth noting that the increase of N improves the MF prediction. Table 3 summarizes the training sets size, the expected value, standard deviation, and associate errors (E) for $N = 1$, 2, and 3. It is worth noting that the MF metamodel with $N = 3$ achieves better results than using $N = 1$ and 2. Furthermore, for $N = 3$ only three evaluations of the highest-fidelity are performed.

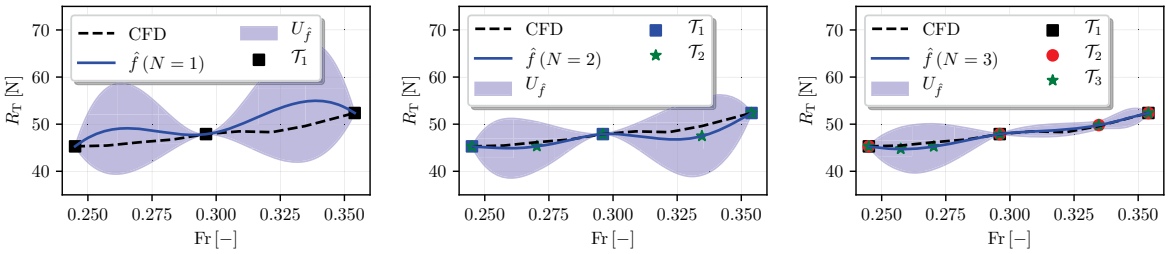

Figure 9: RoPax ferry: model-scale total resistance versus operational uncertainty (Froude number). $N = 1$, 2, and 3 fidelity metamodels.

Table 3: Summary of the adaptive NF metamodel performance on the RoPax UQ problem.

N	$\lvert\mathcal{T}_1\rvert$	$\lvert\mathcal{T}_2\rvert$	$\lvert\mathcal{T}_3\rvert$	Normalized cost	EV	E(EV)%	SD	E(SD)%
1	4			4.0000	48.7053	1.8649	1.3904	-38.1179
2	4		5	4.2500	47.7304	-0.1739	2.1106	-6.0643
3	3	4	6	3.8125	47.7411	-0.1514	2.1953	-2.2977
Reference	9			9	47.8136	-	2.2469	-

7 CONCLUSIONS AND FUTURE WORK

The extension of a two-fidelity metamodel [8] to N-fidelity has been presented for the reduction of the computational cost in solving complex problems by numerical simulations. The method has been tested for an analytical test problem, the simulation-based shape-optimization of a NACA hydrofoil, and the operational-uncertainty quantification of the total resistance of a RoPax ferry at variable advancing speed. The methodology has demonstrated its effectiveness in reducing the computational cost in the problems proposed. For the analytical test problem, the NF method with $N = 3$ has achieved a greater reduction of the highest-fidelity evaluations than with $N = 2$. For the NACA shape-optimization, the NF method with $N = 3$ has achieved comparable solutions to a single-fidelity metamodel, at reduced computational cost. For the operational-uncertainty quantification, the NF method with $N = 3$ has achieved better results than with $N = 1$ and 2, at reduced computational cost. The NACA shape-optimization is likely affected by non-negligible numerical noise for the coarser grids. Therefore, future work will address the presence of numerical noise [16].

ACKNOWLEDGMENTS

CNR-INM is grateful to Dr. Salahuddin Ahmed and Dr. Woei-Min Lin of the Office of Naval Research, for their support through NICOP grant N62909-18-1-2033, and to the Italian Ministry of Education for its support through the Italian Flagship Project RITMARE. The HOLISHIP project (*HOLIstic optimisation of SHIP design and operation for life cycle*, www.holiship.eu) is also acknowledged, funded by the European Union's Horizon 2020 research and innovation programme under grant agreement N. 689074.

REFERENCES

[1] Viana, F. A. C., Simpson, T. W., Balabanov, V. and Vasilli, T. Special section on multidisciplinary design optimization: Metamodeling in multidisciplinary design optimization: How far have we really come?, *AIAA Journal*, **52** (4), 670–690, (2014).

[2] Jin, R., Chen, W. and Simpson, T. W. Comparative studies of metamodelling techniques under multiple modelling criteria, *Structural and Multidisciplinary Optimization*, **23** (1), 1–13, (2001).

[3] Volpi, S., Diez, M., Gaul, N. J., Song, H., Iemma, U., Choi, K. K., Campana, E. F. and Stern, F. Development and validation of a dynamic metamodel based on stochastic radial basis functions and uncertainty quantification, *Structural and Multidisciplinary Optimization*, **51** (2), 347–368, (2015).

[4] Jones, D. R., Schonlau, M. and Welch, W. J. Efficient global optimization of expensive black-box functions, *Journal of Global Optimization*, **13** (4), 455–492, (1998).

[5] Diez, M., Volpi, S., Serani, A., Stern, F. and Campana, E. F., (2019), *Simulation-Based Design Optimization by Sequential Multi-criterion Adaptive Sampling and Dynamic Radial Basis Functions*, pp. 213–228. Springer International Publishing.

[6] Ng, L. W.-T. and Eldred, M. Multifidelity uncertainty quantification using non-intrusive polynomial chaos and stochastic collocation, *53rd AIAA/ASME/ASCE/AHS/ASC Structures, Structural Dynamics and Materials Conference, Structures, Structural Dynamics, and Materials and Co-located Conferences*, (2012).

[7] Baar, J. d., Roberts, S., Dwight, R. and Mallol, B. Uncertainty quantification for a sailing yacht hull, using multi-fidelity kriging, *Computers & Fluids*, **123**, 185 – 201, (2015).

[8] Pellegrini, R., Iemma, U., Leotardi, C., Campana, E. F. and Diez, M. Multi-fidelity adaptive global metamodel of expensive computer simulations, *2016 IEEE Congress on Evolutionary Computation (CEC)*, July, pp. 4444–4451, (2016).

[9] Kuya, Y., Takeda, K., Zhang, X. and Forrester, A. I. J. Multifidelity surrogate modeling of experimental and computational aerodynamic data sets, *AIAA Journal*, **49** (2), 289–298, (2011).

[10] Pellegrini, R., Serani, A., Diez, M., Wackers, J., Queutey, P. and Visonneau, M. Adaptive sampling criteria for multi-fidelity metamodels in CFD-based shape optimization, *7th European Conference on Computational Fluid Dynamics (ECFD 7)*, Glasgow, UK, 11-15 June, (2018).

[11] Queutey, P. and Visonneau, M. An interface capturing method for free-surface hydrodynamic flows, *Computers & Fluids*, **36** (9), 1481–1510, (2007).

[12] Broglia, R. and Durante, D. Accurate prediction of complex free surface flow around a high speed craft using a single-phase level set method, *Computational Mechanics*, **62** (3), 421–437, (2018).

[13] Wackers, J., Deng, G., Guilmineau, E., Leroyer, A., Queutey, P. and Visonneau, M. Combined refinement criteria for anisotropic grid refinement in free-surface flow simulation, *Computers and Fluids*, **92**, 209 – 222, (2014).

[14] Wackers, J., Deng, G., Guilmineau, E., Leroyer, A., Queutey, P., Visonneau, M., Palmieri, A. and Liverani, A. Can adaptive grid refinement produce grid-independent solutions for incompressible flows?, *Journal of Computational Physics*, **344**, 364 – 380, (2017).

[15] Serani, A., Leotardi, C., Iemma, U., Campana, E. F., Fasano, G. and Diez, M. Parameter selection in synchronous and asynchronous deterministic particle swarm optimization for ship hydrodynamics problems, *Applied Soft Computing*, **49**, 313 – 334, (2016).

[16] Wackers, J., Pellegrini, R., Serani, A., Diez, M. and Visonneau, M. Adaptive multifidelity shape optimization based on noisy cfd data, *To be presented at 2019 International Conference on Adaptive Modeling and Simulation (ADMOS 2019)*, El Campello (Alicante), Spain, 27-29 May.